HHS Public Access

Author manuscript

Neuroimage. Author manuscript; available in PMC 2021 January 01.

Published in final edited form as:

Neuroimage. 2020 December ; 223: 117369. doi:10.1016/j.neuroimage.2020.117369.

Nonlinear associations of neurite density and myelin content with age revealed using multicomponent diffusion and relaxometry magnetic resonance imaging

Wenshu Qian, **Nikkita Khattar**, **Luis E. Cortina**, **Richard G. Spencer**[1], **Mustapha Bouhrara**[1,*]

Magnetic Resonance Physics of Aging and Dementia Unit, Laboratory of Clinical Investigations, National Institute on Aging, National Institutes of Health, NIA, NIH, 251 Bayview Blvd., Baltimore, MD 21224, USA

Abstract

Most magnetic resonance imaging (MRI) studies investigating the relationship between regional brain myelination or axonal density and aging have relied upon nonspecific methods to probe myelin and axonal content, including diffusion tensor imaging and relaxation time mapping. While these studies have provided pivotal insights into changes in cerebral architecture with aging and pathology, details of the underlying microstructural alterations have not been fully elucidated. In the current study, we used the BMC-mcDESPOT analysis, a direct and specific multicomponent relaxometry method for imaging of myelin water fraction (MWF), a marker of myelin content, and NODDI, an emerging multicomponent diffusion technique, for neurite density index (NDI) imaging, a proxy of axonal density. We investigated age-related differences in MWF and NDI in several white matter brain regions in a cohort of cognitively unimpaired participants over a wide age range. Our results indicate a quadratic, inverted U-shape, relationship between MWF and age in all brain regions investigated, suggesting that myelination continues until middle age followed by a decrease at older ages, in agreement with previous work. We found a similarly complex regional association between NDI and age, with several cerebral structures also exhibiting a quadratic, inverted U-shape, relationship. This novel observation suggests an increase in axonal density until the fourth decade of age followed by a rapid loss at older ages. We also observed that these age-related differences in MWF and NDI vary across different brain regions, as expected. Finally, our study indicates no significant association between MWF and NDI in most cerebral structures investigated, although this association approached significance in a limited number of brain regions, indicating the complementary nature of their information and encouraging further investigation. Overall, we find evidence of nonlinear associations between age and myelin or axonal density in a sample of well-characterized adults, using direct myelin and axonal content imaging methods.

[*]Corresponding author: bouhraram@mail.nih.gov (M. Bouhrara).

[1]Shared authorship.

Authors contribution

MB: experimental design, WQ, LEC, NK: data preprocessing, WQ, RGS, MB: data analysis, WQ, LEC, NK, RGS, MB: data interpretation, MB: paper drafting, WQ, LEC, NK, RGS, MB: paper editing.

Declaration of Competing Interest

None

Keywords

Myelin water fraction; Axonal density; Normal aging; Quantitative MRI; BMC-mcDESPOT; NODDI

1. Introduction

Biophysical axonal integrity and appropriate myelin content are necessary components for proper central nervous system (CNS) function. Extensive literature has demonstrated a functional and metabolic coupling between these two microstructural components, with loss or degeneration of either compartment may lead to the age-related cognitive decline, motor impairments, and autonomic dysfunction observed in the elderly. Among the numerous age-related alterations observed in the brain parenchyma, myelin loss and axonal damage have been shown to be biological hallmarks of various neurogenerative diseases such as multiple sclerosis and dementia (MacKay et al., 2009, Bouhrara et al., 2018, Bartzokis, 2011, Medana et al., 2003). However, the mechanisms underlying these cerebral microstructural changes remain poorly understood. Therefore, it is crucial to characterize changes in myelin content and axonal density that occur with normal aging and in the absence of clinically detectable pathology, to identify alterations that originate from pathological processes. Indeed, throughout the lifespan, the human brain experiences notable structural alterations in white matter (WM) and gray matter (GM). Postmortem histological studies have shown that myelin and axonal degeneration are among the main sequelae of aging and may be associated with concomitant motor and cognitive decline, as well as likely being closely linked to a myriad of age-associated neurodegenerative disorders and dementias (Flynn et al., 2003, Kolasinski et al., 2012, Bronge et al., 2002, Pannese, 2011, Stassart et al., 2018, Tang et al., 1997, Marner et al., 2003). Although histologic preparations have provided invaluable insight into normal brain aging, this method is available only for post-mortem studies, while a great deal interest attaches to longitudinal evaluation of brain aging. Thus, there remains a great deal of interest in non-invasive investigation of human brain microstructure.

Magnetic resonance imaging (MRI) has been widely used in clinical and preclinical investigations of the brain, and has provided pivotal data characterizing structural and functional cerebral changes with disease and aging (Gunning-Dixon et al., 2009). Parameters derived from diffusion tensor imaging (DTI) in particular, along with, to a lesser extent, relaxation time imaging, have been found to follow complex and nonlinear trajectories with age in WM and GM (Inano et al., 2011, Bartzokis et al., 2003, Yeatman et al., 2014, Fjell et al., 2009, Arshad et al., 2016, Sullivan and Pfefferbaum, 2006, Saito et al., 2009). However, the underlying structural mechanisms responsible for these findings are difficult to define due to the sensitivity of conventional MRI indices to a number of tissue properties, including hydration, macromolecular content, axonal density, myelin content, iron content, and architectural features such as fiber crossing and fanning. To address these limitations, more advanced analysis methods based on multicomponent relaxometry or diffusion have been introduced to improve both sensitivity and specificity of MR-based myelination and axonal density studies (MacKay et al., 1994, MacKay and Laule, 2016, Laule et al., 2008, Laule et

al., 2006). Using multicomponent relaxometry analysis, Mackay and colleagues pioneered *in-vivo* MR imaging of myelin water fraction (MWF) (MacKay et al., 1994, MacKay and Laule, 2016), which has been histologically validated as a proxy for myelin content (Laule et al., 2008, Laule et al., 2006). This approach has been extensively applied to characterize cerebral demyelinating diseases and neurodevelopment (Bouhrara et al., 2018, Flynn et al., 2003, Borich et al., 2013, Laule et al., 2004, Sirrs et al., 2007, Dean et al., 2017, Bouhrara et al., 2015). However, multicomponent relaxometry is unable to distinguish between intracellular water fraction, a proxy of axonal density, and extracellular water fraction due to their similar relaxation times. To overcome this difficulty, Zhang and colleagues have introduced a new multicomponent diffusion technique to map intracellular water in brain, called neurite orientation dispersion and density imaging (NODDI) (Zhang et al., 2012). NODDI is based on a compartmental model of water diffusion incorporating intracellular water, that is, water within neurites, extracellular water, and a compartment consisting of less restricted water from the cerebral spinal fluid volume. NODDI has gained rapid popularity and has been shown to provide reliable and specific information about neurite density and dispersion in studies of aging (Kunz et al., 2014, Billiet et al., 2015, Chang et al., 2015, Nazeri et al., 2015, Merluzzi et al., 2016, Kodiweera et al., 2016, Grussu et al., 2015, Jelescu et al., 2015, Grussu et al., 2017), as well as in investigations of neurologic disorders (Timmers et al., 2016, Timmers et al., 2015, Mitchell et al., 2019, Churchill et al., 2017, Churchill et al., 2019, By et al., 2017, Adluru et al., 2014, Winston et al., 2014, Wen et al., 2015).

To the best of our knowledge, only a single pioneering study has sought to jointly investigate alterations in myelin content and axonal density with age through a combination of multicomponent relaxometry and diffusion analysis (Billiet et al., 2015). Based on multi-echo imaging for MWF mapping and NODDI for neurite density index (NDI) imaging, Billiet and colleagues observed increases in NDI with age in several cerebral WM regions. While their observations agree with those of Chang and colleagues, (Billiet et al., 2015, Chang et al., 2015), they do not support Merluzzi and colleagues' observation of decreased NDI in different cerebral WM structures (Merluzzi et al., 2016). This discrepancy may be attributable to differences in the study cohorts. In addition, and surprisingly, Billiet's study showed no difference in MWF with age; this disagrees with various MWF-based studies revealing a quadratic, inverted U-shaped, association between MWF and age in WM (Arshad et al., 2016, Bouhrara et al., 2020a, Bouhrara et al., 2020b). It remains unclear whether this discrepancy is due to differences in cohort characteristics or the MR methodology used to measure MWF, emphasizing the need for additional studies.

In the current study, we investigated the pattern of myelination and axonal density in normative aging in a cohort of well-characterized cognitively unimpaired participants (n = 58), across the extended age range of 21 to 83 years. Our measure of MWF was conducted using the Bayesian Monte Carlo analysis of multi-component driven equilibrium single-component observation of T_1 and T_2 (BMC-mcDESPOT) method (Bouhrara and Spencer, 2016, Bouhrara and Spencer, 2017). BMC-mcDESPOT generates a high-resolution whole brain MWF map with high accuracy and precision, and has been previously applied to provide evidence of myelin loss in mild cognitive impairment and dementia and to investigate brain myelin maturation and aging as well as the association between cerebral

blood flow and myelin content (Bouhrara et al., 2018, Bouhrara et al., 2020a, Bouhrara et al., 2020b, Bouhrara et al., 2020c). Our measure of NDI was conducted using the NODDI approach (Zhang et al., 2012). Our main goals are to characterize age-related differences in regional brain myelination and axonal density, to investigate the association between MWF and NDI, to provide further insights into regional brain maturation and aging over the adult lifespan, and to demonstrate the feasibility and utility of combining NODDI and BMC-mcDESPOT for advanced clinical investigations.

2. Materials and methods

2.1. Participants

Participants were drawn from two ongoing healthy aging cohorts of the National Institute on Aging (NIA). Eleven volunteers recruited from the Baltimore Longitudinal Study of Aging (BLSA) (Shock, 1985, Ferrucci, 2008), and forty seven from the Genetic and Epigenetic Signatures of Translational Aging Laboratory Testing (GESTALT) were enrolled. The study populations, experimental design, and measurement protocols of the BLSA have previously been reported (Shock, 1985, Ferrucci, 2008). The BLSA is a longitudinal cohort study funded and conducted by the National Institute on Aging (NIA) Intramural Research Program (IRP). Established in 1958, the BLSA enrolls community-dwelling adults with no major chronic conditions or functional impairments at enrollment. The GESTALT study is also a study of healthy volunteers, initiated in 2015 and funded and conducted by the NIA IRP. The goal of the BLSA and GESTALT studies is to evaluate multiple biomarkers related to aging. We note that the inclusion and exclusion criteria for these two studies are essentially identical. Participants underwent testing at the NIA's clinical research unit and were excluded if they had metallic implants, neurologic, or significant medical disorders. In addition, all participants underwent a Mini Mental State Examination (MMSE). The final cohort consisted of 58 cognitively unimpaired volunteers (mean ± standard deviation MMSE = 29.2 ± 1.0) ranging in age from 21 to 83 years (45.4 ± 18.3 years), including 31 men (42.9 ± 17.5 years) and 27 women (48.3 ± 19.1 years). Age and MMSE did not differ significantly between men and women. Experimental procedures were performed in compliance with our local Institutional Review Board, and participants provided written informed consent.

2.2. Data acquisition

All experiments were performed with a 3T whole body Philips MRI system (Achieva, Best, The Netherlands) using the internal quadrature body coil for transmission and an eight-channel phased-array head coil for reception. We emphasize that all MRI studies and ancillary measurements were performed with the same MRI system, running the same pulse sequences, at the same facility, and directed by the same investigators for both BLSA and GESTALT participants.

2.2.1. NODDI for NDI mapping—Diffusion-weighted images (DWI) were acquired using a single-shot echo planar imaging sequence: repetition time (TR) / echo time (TE) of 10000 / 67 ms, two b-values of 700 and 2000 s/mm^2, each encoded in 32 diffusion-weighting gradient directions, two images with b of 0 s/mm^2, field-of-view (FoV) of 240 mm × 208 mm × 150 mm, acquisition matrix of 120 × 120 × 50, acquisition voxel size of 2

mm × 2 mm × 3 mm, and SENSE factor of 2. All images were reconstructed to a voxel size of 2 mm × 2 mm × 2 mm. The total acquisition time was ~12 min.

2.2.2. BMC-mcDESPOT for MWF mapping—3D spoiled gradient recalled echo (SPGR) images were acquired with flip angles (FAs) of [2 4 6 8 10 12 14 16 18 20]°, TR/TE of 5/1.37 ms, and acquisition time of 5 min, as well as 3D balanced steady state free precession (bSSFP) images were acquired with FAs of [2 4 7 11 16 24 32 40 50 60]°, TR/TE of 5.8/2.8 ms, and acquisition time of ~6 min. The bSSFP images were acquired with radiofrequency excitation pulse phase increments of 0 or π in order to account for off-resonance effects (Deoni, 2011). All SPGR and bSSFP images were acquired with matrix size of 150 × 130 × 94, acquisition voxel size of 1.6 mm × 1.6 mm × 1.6 mm, and SENSE factor of 2. Further, the double-angle method (DAM) was used to correct for excitation radio frequency inhomogeneity (Stollberger and Wach, 1996). This makes use of two fast spin-echo images acquired with flip angles of 45° and 90°, TR/TE of 3000/102 ms, acquisition voxel size of 2.6 mm × 2.6 mm × 4 mm, and acquisition time of ~4 min. All images were acquired with FOV of 240 mm × 208 mm × 150 mm and reconstructed to a voxel size of 2 mm × 2 mm × 2 mm. The total acquisition time was ~21 min.

2.3. NDI and MWF mapping

For each participant, an NDI map was generated using the NODDI analysis as described previously (Zhang et al., 2012). Specifically, all DW images were registered to the averaged b_0 image and corrected for motion and eddy current distortion artifacts using the Artefact Correction in Diffusion MRI (ACID) toolbox (http://diffusiontools.com/) (Mohammadi et al., 2010). The NODDI analysis was conducted on the registered images using the NODDI toolbox (https://www.nitrc.org/projects/noddi_toolbox), a multi-shell diffusion analysis package which enables the estimation of three separate water compartments, namely intracellular (*i.e.* NDI), extracellular, and cerebrospinal fluid.

Using the FSL software, all SPGR, bSSFP, and DAM images for each participant were linearly registered to the SPGR image acquired at FA of 10°, and the derived transformation matrix was then applied to the original SPGR, bSSFP, and DAM images. A MWF map was then generated using the BMC-mcDESPOT analysis from the registered SPGR, bSSFP, and DAM datasets (Bouhrara and Spencer, 2016, Bouhrara and Spencer, 2017). Briefly, BMC-mcDESPOT assumes a two-component system consisting of a short relaxation component, corresponding to the signal of water trapped within the myelin sheets, and a long relaxation component, corresponding to intra/extra cellular water. Analysis was performed explicitly accounting for nonzero TE as incorporated into the TE-corrected-mcDESPOT signal model (Bouhrara and Spencer, 2015).

2.4. Regions-of-interest segmentation

The averaged SPGR image over FAs for each participant was registered using nonlinear registration to the Montreal Neurological Institute (MNI) standard space image and the derived transformation matrix was then applied to the MWF map for that participant. Similarly, the averaged DW image obtained with b of 0 was registered using nonlinear registration to the MNI image and the derived transformation matrix was then applied to the

NDI map. Twenty-one WM regions of interest (ROIs) were defined from the MNI structural atlas and the Johns Hopkins University ICM-DTI-81 atlas, including: whole brain (WB) WM, frontal lobes (FL) WM, parietal lobes (PL) WM, temporal lobes (TL) WM, occipital lobes (OL) WM, cerebellum (CRB) WM, body of corpus callosum (BCC), genu of corpus callosum (GCC), splenium of corpus callosum (SCC), internal capsules (IC), cerebral peduncle (CP), anterior corona radiata (ACR), posterior corona radiata (PCR), anterior thalamic radiation (ATR), posterior thalamic radiation (PTR), inferior fronto-occipital fasciculus (IFOF), superior fronto-occipital fasciculus (SFOF), inferior longitudinal fasciculus (ILF), superior longitudinal fasciculus (SLF), forceps minor (Fm), and forceps major (FM). All ROIs were eroded to reduce partial volume effects and imperfect image registration using the FSL tool *fslmaths.* Finally, the mean MWF and NDI values in each ROI of each participant were calculated.

2.5. Statistical analysis

To investigate the effects of age and sex on MWF and NDI, multi linear regression was applied using the mean MWF or NDI within each ROI as the dependent variable and sex, age, and age^2 as the independent variables, after mean age centering. Mean age centering was performed by subtracting the mean age value calculated over all subjects from the age of each subject. In all cases, the interactions between sex and age or age^2 were found to be non-significant and were therefore omitted from the model. The threshold for statistical significance was $p < 0.05$ after correction for multiple ROI comparisons using the false discovery rate (FDR) method (Benjamini, 2010, Benjamini and Hochberg, 1995).

Moreover, for each ROI, ANOVA analysis was performed to test for differences between mean MWF or NDI values averaged over participants within the age intervals of 20–29, 30–49, 50–69, and 70–89 years. Post-hoc Bonferroni correction was applied at the significance level of 0.1 to account for multiple comparisons across age intervals.

Further, for each ROI, Pearson correlation was conducted to examine the relationships between NDI and MWF. Finally, we investigated the association between NDI and MWF using multi linear regression analysis with the mean NDI within each ROI as the dependent variable and the MWF within the ROI, age, and sex as the independent variables. The threshold for statistical significance was $p < 0.05$ after correction for multiple ROI comparisons using the FDR method.

All analyses were performed using MATLAB (MathWorks, Natick, MA, USA).

3. Results

Figs. 1 and 2 show average NDI or MWF maps by age decade over the adult lifespan for three representative axial slices. Visual inspection indicates increases in NDI or MWF values from early adulthood through middle age (*i.e.* 40–49 years), followed by reduced NDI or MWF in several brain regions, consistent with progressive increases in myelin content or axonal density followed by reductions at older ages. Furthermore, we note that different regions exhibit different patterns in the association of NDI or MWF with age, with the

parietal lobes exhibiting greater NDI values while the occipital and parietal lobes exhibiting greater MWF as compared to the more anterior brain regions.

Figs. 3 and 4 show, respectively, quantitative results for NDI and MWF values from all participants as a function of age for the indicated 21 WM regions. These results show increasing NDI or MWF until middle age followed by decreases in NDI or MWF with age in most examined ROIs, in agreement with Figs. 1 and 2. The best-fit curves indicate that while the fundamental inverted U-shaped relationship between NDI or MWF and age was consistent across all ROIs, the age curves displayed regional variation. Furthermore, in agreement with Fig. 2, the highest MWF values were found in the occipital and parietal lobes, with the frontal and temporal lobes exhibiting overall lower MWF values, while for NDI, the highest values were seen in the parietal lobes, in agreement with Fig. 1.

Our statistical analysis, presented in Table 1, showed significant effects of age on NDI in four of the brain regions evaluated, namely, the cerebellum, genu of CC, cerebral peduncles, and forceps major (Table 1). Here, the effect of age on NDI in the anterior corona radiata, superior fronto-occipital fasciculus, and forceps minor was significant before FDR correction. Similarly, the quadratic effect of age, age^2, was significant ($p < 0.05$) or close to significance ($p < 0.1$) in various brain structures (Table 1). Here, the effect of age^2 on NDI in the occipital lobes, superior longitudinal fasciculus, and forceps major was significant before FDR correction. Moreover, our statistical analyses indicate that all ROIs exhibited non-significant interactions between age^2 and sex or age and sex on NDI. Sex effect on NDI was not significant in any of the ROIs. However, the genu of CC, longitudinal fasciculus, and forceps exhibited a significant sex effect before FDR. In these brain regions, women had 2 to 6 % higher NDI values than men. Furthermore, the effect of age on MWF was significant or close to significance in several ROIs while the quadratic effect of age, age^2, was significant or close to significance in all ROIs except the genu of CC (Table 1). Moreover, our statistical analyses indicate that all ROIs exhibited non-significant interactions between age^2 and sex or age and sex on MWF. Sex effect on MWF was not significant in any ROI. However, the parietal lobes, splenium, and forceps major all exhibited a close to significant effect of sex before FDR. In these brain regions, women had ~8% higher MWF values than men. Finally, for each ROI exhibiting significant age^2 effect, we determined the specific year at which MWF or NDI peaked (Table 1). As seen, the MWF of the occipital lobes, parietal lobes, cerebral peduncles, and cerebellum reached a maximum at later ages as compared to all other WM structures, while the parietal lobes, internal capsules, and superior fronto-occipital fasciculus reached a maximum NDI at later ages as compared to other WM structures.

The ANOVA analysis comparing the regional mean NDI or mean MWF values averaged over participants within age intervals indicated that for most ROIs (Fig. 5), there was a statistically significant variation in NDI or MWF values across age intervals. The post hoc analysis indicated that significance was mainly between age-intervals 20–29, 30–49, or 50–69 and 70–89.

Finally, Fig. 6 shows the weak Pearson correlations between MWF and NDI for all ROIs. The nominal significance in occipital and temporal lobes, and genu of corpus callosum did

not survive the FDR correction. This illustrates the unique information these metrics provide and highlights the potential of NODDI and BMC-mcDESPOT to provide complementary insights. Finally, the association between NDI and MWF while accounting for age and sex as covariates indicated significant associations in several brain structures, namely, the whole brain, occipital lobes, temporal lobes, genu of CC, and inferior longitudinal fasciculus. However, significance did not survive FDR correction.

4. Discussion

In this cross-sectional study, we investigated the association between NDI, a measure of neurite density, and MWF, a measure of myelin content, and age in several cerebral WM structures in a healthy adult population spanning a wide age range. NDI was derived from NODDI (Zhang et al., 2012), a multicomponent diffusion analysis method, while MWF was derived from BMC-mcDESPOT, a multicomponent relaxometry method (Bouhrara and Spencer, 2016, Bouhrara and Spencer, 2017). Our results revealed widespread WM microstructural differences as a function of age as well as regional variations between the NDI and MWF measures; we attribute this to different aspects of microstructural changes over adulthood.

In most of the cerebral structures examined, we observed a quadratic, inverted U-shaped, association between NDI and age (Fig. 3). Although this relationship was statistically significant in a limited number of brain structures (Table 1), it likely reflects an increase in axonal density throughout young to middle age and a decrease afterwards. These results may help to some extent in reconciling the apparent discrepancies in NDI results in the literature. Indeed, in pioneering studies, Billiet and colleagues and Chang and colleagues have observed increases in NDI with age in a number of cerebral WM regions (Billiet et al., 2015, Chang et al., 2015), while Merluzzi and colleagues observed decreases in NDI in several WM regions (Merluzzi et al., 2016). However, the age range of the cohorts in these studies was relatively limited. Although Billiet's study incorporated a wide age range, it did not include subjects above the age of 70 and incorporates only a few subjects over 60 years, while Chang's cohort was composed primarily of relatively young subjects in the age range of 7–63. Finally, Merluzzi's cohort included only subjects over 45 years. These limitations in previous studies may have precluded detection of the nonlinear, more biologically plausible, associations of NDI with age that we observed. Indeed, nonlinear patterns with age in various WM brain structures (Inano et al., 2011, Bartzokis et al., 2003, Yeatman et al., 2014, Fjell et al., 2009, Arshad et al., 2016, Sullivan and Pfefferbaum, 2006, Saito et al., 2009) have been found using conventional quantitative MRI methods. However, while these previous studies may provide some experimental support to our observation, we note that conventional MRI measures, although sensitive to axonal water signal, are also sensitive to a number of tissue properties, including hydration, macromolecular content, iron content, myelin content, and architectural features such as fiber crossing and fanning, rendering them nonspecific to any underlying tissue propriety. Furthermore, it must be recognized recognized that other technical factors may have contributed further to the discrepancy between studies, including our current investigation, such as differences in acquisition parameters, cohort sizes, image manipulations (for example, image registration and segmentation), and statistical methods. As an example, the NODDI model does not

explicitly account for different transverse relaxation times in different tissue compartments; this makes it highly echo-time-dependent; this has been shown to significantly bias NODDI-derived measures, including NDI (Gong et al., 2020). Another potential source of discrepancy is the dependence of the statistical models adopted on the variables used in the final regression model. Finally, the specific values of NDI and MWF parameters, their significance, and trends with age will exhibit some variability as a function of sampling density within age groups, range of ages incorporated, and consistency of data (Fjell et al., 2010).

In agreement with previous work, our results indicate a significant quadratic association between MWF and age in most cerebral WM regions examined (Fig. 4). These results are consistent with Arshad and colleagues' and Bouhrara and colleagues' recent studies indicating an inverted U-shape pattern of MWF values with age in different WM regions (Arshad et al., 2016, Bouhrara et al., 2020a). The quadratic association between MWF and age is attributed to the process of myelination from youth through middle age, followed by demyelination in later years (Arshad et al., 2016, Bouhrara et al., 2020a, Bartzokis et al., 2010); this pattern is in agreement with postmortem observations (Tang et al., 1997, Peters, 2002). As expected, we found that different regions exhibit both similarities and differences in associations between MWF and age, with most regions peaking at the fifth life decade with the occipital and parietal lobes exhibited delayed demyelination as compared to the other lobes. This pattern is consistent with the retrogenesis hypothesis (first in-last out), in which posterior brain regions are spared from degeneration as compared to anterior brain regions (Stricker et al., 2009, Brickman et al., 2012, Raz, 2000, Bender et al., 2016). These findings are consistent with studies based on myelin-sensitive, but nonspecific, MRI methods such as DTI and relaxation times (Yeatman et al., 2014, Saito et al., 2009, Bartzokis et al., 2010, Okubo et al., 2017, Westlye et al., 2010), and strongly motivate additional longitudinal studies.

In contrast to De Santis and colleagues' observation (De Santis et al., 2014), our results did not find a significant correlation between NDI and MWF in any of the 21 ROIs studied (Fig. 6). This discrepancy is likely due to several methodological factors. First, unlike our study, De Santis and colleagues' study was conducted in a small cohort size ($N = 17$) spanning a limited age range of young subjects (mean age = 24.2 ± 2.8 years). Second, in their study, axonal density was estimated from the composite hindered and restricted model of diffusion, CHARMED (Assaf and Basser, 2005). There are fundamental differences between the NODDI and CHARMED models (Winston, 2015). One important example is that the NODDI signal model incorporates three compartments while CHARMED incorporates only two. Further, in NODDI, the intracellular component is modelled as sticks with orientation approximated using the Watson distribution to account for dispersion, while CHARMED does not model orientation dispersion, which can lead to an underestimation of axonal density. Further, while in both methods the extracellular component is modelled by anisotropic Gaussian diffusion, NODDI incorporates a third component corresponding to cerebrospinal fluid modelled by isotropic diffusion. Lastly, De Santi and colleagues used conventional mcDESPOT to map MWF (Deoni et al., 2008); parameter estimates obtained in this way can show a great deal of variability with respect to noise (Bouhrara et al., 2016, Lankford and Does, 2013, West et al., 2019). Our Bayesian implementation greatly

stabilizes these parameter estimates, thereby permitting markedly improved MWF determination (Bouhrara and Spencer, 2016, Bouhrara and Spencer, 2017).

Some of the WM brain structures studied exhibited a potential association between NDI and MWF after controlling for age and sex in the multi-linear regression analysis. However, this association did not survive FDR correction. This could be due to study characteristics, including a potentially underpowered study or lack of availability of very young participants (<20 years old) in accordance with the inclusion and exclusion criteria of the BLSA and GESTALT studies. Indeed, studies have shown that myelination is in part modulated by axonal activity (Mensch et al., 2015, Wake et al., 2011). Moreover, aside from acting as an electric insulator, oligodendrocytes, the cells that produce and maintain myelin, may provide substantial metabolic support to underlying axons (Simons and Nave, 2015). However, other facts argue against an association between NDI and MWF, including the fact that a numerical majority of cerebral axons are unmyelinated (Stassart et al., 2018), in addition to the appearance of tiny axons at older ages (Marner et al., 2003). Further, some studies suggest that myelin loss does not lead to axonal degeneration in a long-lived model of chronic demyelination (Smith et al., 2013). Therefore, it remains unclear whether the maturation of axons and of the myelination pattern of the brain are mechanistically associated or represent two independent neurological processes. In terms of degenerative processes, increasing evidence suggest that axonal degeneration occurs before the onset of clinical symptoms in several age-related diseases including dementias (Kanaan et al., 2013). However, as for multiple sclerosis, it is unclear whether axonal damage is independent of, or secondary to, demyelination in dementia. Further studies probing changes in myelin and axonal content using larger cohorts, and especially longitudinal studies, are required to fully elucidate the relationship between axonal density and myelin. These studies will be of critical importance for the development of specific therapeutic strategies supporting myelin and axonal simultaneous homeostatic phenotype.

Our calculated NDI and MWF mean values were overall in good agreement with those previously reported (Arshad et al., 2016, MacKay and Laule, 2016, Dean et al., 2017, Billiet et al., 2015, Chang et al., 2015, Merluzzi et al., 2016, Dvorak et al., 2019). However, we note that mcDESPOT, including BMC-mcDESPOT, provides somewhat higher MWF values as compared to multiple spin echo (MSE)-based methods (Zhang et al., 2015). Indeed, various experimental and physiological factors that are not incorporated into the MSE or mcDESPOT signal models could account for this discrepancy. This includes, but is not limited to, magnetization transfer between macromolecules and free water protons, longitudinal relaxation time effects resulting from use of short repetition times in MSE, exchange between water pools, *J*-coupling, off-resonance, spin locking, water diffusion within different compartments, and internal gradients. Further, as noted above, NDI measures from NODDI are biased due to T_2-weighting that is not accounted for in the underlying signal model (Gong et al., 2020). In addition, the intrinsic diffusivity for NODDI is fixed to 1.7 $\mu m^2/ms$ (Zhang et al., 2012). Although this value has been shown to be appropriate for adult brain WM, it has also been demonstrated that it is likely to be an overestimate for adult brain gray matter (GM) or infant brain WM and GM (Guerrero et al., 2019). These represent major challenges in MR imaging studies of myelin content and

axonal density, and further technical developments are required to improve accuracy of both myelin content and axonal density imaging.

Although our work used advanced methodology, certain limitations remain. While our cohort spanned a wide age range, it does not include very young participants (< 20 years old), due to the inclusion and exclusion criteria of the BLSA and GESTALT studies. Inclusion of younger participants may influence the shape of MWF and NDI age-related trajectories (Fjell et al., 2010) and the assessment of their maxima with respect to age. We also note that it was not feasible to obtain optimal uniform sampling across all age intervals in this convenience sample of participants in ongoing research protocols, although all decades were well-represented. Moreover, our dataset is cross-sectional, so that the quadratic trends with age observed here require further validation through longitudinal studies. Such work, motivated by the present results, is underway. Finally, our work did not investigate differences with age or sex in MWF or NDI in GM regions; this was due to the facts that NDI determination using NODDI has been found to be unreliable in GM regions (Guerrero et al., 2019), while accurate determination of MWF in GM is highly problematic due to the small amount of myelin in GM (Bonny et al., 2020, Bouhrara et al., 2018).

5. Conclusions

In this cross-sectional study examining sex differences and age-related alterations in neurite density and myelination across a wide age range of cognitively normal subjects, we showed that both neurite density and myelination in most ROIs studied follow complex patterns with age described by quadratic, inverted U-shape, relationships. Further, our results indicate that NODDI and BMC-mcDESPOT MRI provide complementary information regarding white matter integrity, and may be combined to investigate the underlying mechanisms of axonal and myelin damage in neurodevelopment and neurodegeneration.

Acknowledgement

This work was supported by the Intramural Research Program of the National Institute on Aging of the National Institutes of Health. We gratefully acknowledge Christopher M. Bergeron, Denise Melvin, and Linda Zukley for their assistance with data acquisition and participant recruitment and logistics.

References

Adluru G, Gur Y, Anderson JS, Richards LG, Adluru N, DiBella EV, 2014 Assessment of white matter microstructure in stroke patients using NODDI. Conf Proc IEEE Eng Med Biol Soc 2014, 742–745.

Arshad M, Stanley JA, Raz N, 2016 Adult age differences in subcortical myelin content are consistent with protracted myelination and unrelated to diffusion tensor imaging indices. Neuroimage 143, 26–39. [PubMed: 27561713]

Assaf Y, Basser PJ., 2005 Composite hindered and restricted model of diffusion (CHARMED) MR imaging of the human brain. NeuroImage 27 (1), 48–58. [PubMed: 15979342]

Bartzokis G, Cummings JL, Sultzer D, Henderson VW, Nuechterlein KH, Mintz J, 2003 White matter structural integrity in healthy aging adults and patients with Alzheimer disease: a magnetic resonance imaging study. Arch. Neurol 60 (3), 393–398. [PubMed: 12633151]

Bartzokis G, Lu PH, Tingus K, Mendez MF, Richard A, Peters DG, et al., 2010 Lifespan trajectory of myelin integrity and maximum motor speed. Neurobiol. Aging 31 (9), 1554–1562. [PubMed: 18926601]

Bartzokis G, 2011 Alzheimer's disease as homeostatic responses to age-related myelin breakdown. Neurobiol. Aging 32 (8), 1341–1371. [PubMed: 19775776]

Bender AR, Völkle MC, Raz N, 2016 Differential aging of cerebral white matter in middle-aged and older adults: a seven-year follow-up. NeuroImage 125, 74–83. [PubMed: 26481675]

Benjamini Y, Hochberg Y, 1995 Controlling the false discovery rate: a practical and powerful approach to multiple testing. J. R. Stat. Soc. Series B (Methodol.) 57 (1), 289–300.

Benjamini Y, 2010 Discovering the false discovery rate. J. R. Stat. Soc. Series B (Stat. Methodol.) 72 (4), 405–416.

Billiet T, Vandenbulcke M, Madler B, Peeters R, Dhollander T, Zhang H, et al., 2015 Age-related microstructural differences quantified using myelin water imaging and advanced diffusion MRI. Neurobiol. Aging 36 (6), 2107–2121. [PubMed: 25840837]

Billiet T, Vandenbulcke M, Mädler B, Peeters R, Dhollander T, Zhang H, et al., 2015 Age-related microstructural differences quantified using myelin water imaging and advanced diffusion MRI. Neurobiol. Aging 36 (6), 2107–2121. [PubMed: 25840837]

Bonny J-M, Traore A, Bouhrara M, Spencer RG, Pages G, 2020 Parsimonious discretization for characterizing multi-exponential decay in magnetic resonance. NMR Biomed e4366. [PubMed: 32789944]

Borich MR, MacKay AL, Vavasour IM, Rauscher A, Boyd LA, 2013 Evaluation of white matter myelin water fraction in chronic stroke. NeuroImage: Clin 2, 569–580. [PubMed: 24179808]

Bouhrara M, Rejimon AC, Cortina LE, Khattar N, Bergeron CM, Ferrucci L, et al., 2020a Adult brain aging investigated using BMC-mcDESPOT based myelin water fraction imaging. Neurobiol. Aging 85, 131–139. [PubMed: 31735379]

Bouhrara M, Cortina LE, Rejimon AC, Khattar N, Bergeron C, Bergeron J, et al., 2020b Quantitative age-dependent differences in human brainstem myelination assessed using high-resolution magnetic resonance mapping. NeuroImage 206, 116307. [PubMed: 31669302]

Bouhrara M, Alisch J, Nikkita N, Kim R, Rejimon A, Cortina L, et al., 2020c Association of cerebral blood flow with myelin content in cognitively unimpaired adults. BMJ Neurol. Open 2, e000053.

Bouhrara M, Reiter D, Bergeron C, Zukley L, Ferrucci L, Resnick S, et al., 2018 Evidence of demyelination in mild cognitive impairment and dementia using a direct and specific magnetic resonance imaging measure of myelin content. Alzheimer's Dementia 14 (8), 998–1004.

Bouhrara M, Reiter DA, Celik H, Fishbein KW, Kijowski R, Spencer RG, 2016 Analysis of mcDESPOT- and CPMG-derived parameter estimates for two-component nonexchanging systems. Mag. Resonance Med 75 (6), 2406–2420.

Bouhrara M, Reiter DA, Maring MC, Bonny JM, Spencer RG, 2018 Use of the NESMA filter to improve myelin water fraction mapping with brain MRI. J. Neuroimaging 28 (6), 640–649. [PubMed: 29999204]

Bouhrara M, Reiter DA, Spencer RG, 2015 Bayesian analysis of transverse signal decay with application to human brain. Magn. Resonance Med 74 (3), 785–802.

Bouhrara M, Spencer RG., 2015 Incorporation of nonzero echo times in the SPGR and bSSFP signal models used in mcDESPOT. Magn. Reson. Med 74 (5), 1227–1235. [PubMed: 26407635]

Bouhrara M, Spencer RG., 2016 Improved determination of the myelin water fraction in human brain using magnetic resonance imaging through Bayesian analysis of mcDESPOT. NeuroImage 127, 456–471. [PubMed: 26499810]

Bouhrara M, Spencer RG., 2017 Rapid simultaneous high-resolution mapping of myelin water fraction and relaxation times in human brain using BMC-mcDESPOT. NeuroImage 147, 800–811. [PubMed: 27729276]

Brickman AM, Meier IB, Korgaonkar MS, Provenzano FA, Grieve SM, Siedlecki KL, et al., 2012 Testing the white matter retrogenesis hypothesis of cognitive aging. Neurobiol. Aging 33 (8), 1699–1715. [PubMed: 21783280]

Bronge L, Bogdanovic N, Wahlund LO, 2002 Postmortem MRI and histopathology of white matter changes in Alzheimer brains. Dementia Geriatric Cogn. Disord 13 (4), 205–212.

By S, Xu J, Box BA, Bagnato FR, Smith SA, 2017 Application and evaluation of NODDI in the cervical spinal cord of multiple sclerosis patients. Neuroimage Clin 15, 333–342. [PubMed: 28560158]

Chang YS, Owen JP, Pojman NJ, Thieu T, Bukshpun P, Wakahiro ML, et al., 2015 White matter changes of neurite density and fiber orientation dispersion during human brain maturation. PLoS One 10 (6), e0123656. [PubMed: 26115451]

Chang YS, Owen JP, Pojman NJ, Thieu T, Bukshpun P, Wakahiro MLJ, et al., 2015 White matter changes of neurite density and fiber orientation dispersion during human brain maturation. PloS One 10 (6), e0123656. [PubMed: 26115451]

Churchill NW, Caverzasi E, Graham SJ, Hutchison MG, Schweizer TA, 2017 White matter microstructure in athletes with a history of concussion: comparing diffusion tensor imaging (DTI) and neurite orientation dispersion and density imaging (NODDI). Hum. Brain Mapp 38 (8), 4201–4211. [PubMed: 28556431]

Churchill NW, Caverzasi E, Graham SJ, Hutchison MG, Schweizer TA, 2019 White matter during concussion recovery: comparing diffusion tensor imaging (DTI) and neurite orientation dispersion and density imaging (NODDI). Hum. Brain Mapp 40 (6), 1908–1918. [PubMed: 30585674]

De Santis S, Drakesmith M, Bells S, Assaf Y, Jones DK, 2014 Why diffusion tensor MRI does well only some of the time: variance and covariance of white matter tissue microstructure attributes in the living human brain. Neuroimage 89, 35–44. [PubMed: 24342225]

Dean DC 3rd, Hurley SA, Kecskemeti SR, O'Grady JP, Canda C, Davenport-Sis NJ, et al., 2017 Association of amyloid pathology with myelin alteration in preclinical Alzheimer disease. JAMA Neurol 74 (1), 41–49. [PubMed: 27842175]

Deoni SC, Rutt BK, Arun T, Pierpaoli C, Jones DK, 2008 Gleaning multicomponent T1 and T2 information from steady-state imaging data. Magn. Resonance Med 60 (6), 1372–1387.

Deoni SC., 2011 Correction of main and transmit magnetic field (B0 and B1) inhomogeneity effects in multicomponent-driven equilibrium single-pulse observation of T1 and T2. Magn. Resonance Med 65 (4), 1021–1035.

Deoni SC., 2019 Multivariate template creation of a myelin water brain atlas with GRASE and mcDESPOT In: Dvorak A, Liu H, Ljungberg E, Vavasour I, Lee L, MacKay A, et al. (Eds.), Proceedings of the International Society for Magn. Resonance Med. (ISMRM), Canada.

Ferrucci L, 2008 The Baltimore Longitudinal Study of Aging (BLSA): a 50-year-long journey and plans for the future. J. Gerontol. Series A Biol. Sci. Med. Sci 63 (12), 1416–1419.

Fjell AM, Engvig A, Tamnes CK, Grydeland H, Walhovd KB, Westlye LT, et al., 2009 Life-span changes of the human brain white matter: diffusion tensor imaging (DTI) and volumetry. Cerebral Cortex 20 (9), 2055–2068. [PubMed: 20032062]

Fjell AM, Walhovd KB, Westlye LT, Ostby Y, Tamnes CK, Jernigan TL, et al., 2010 When does brain aging accelerate? Dangers of quadratic fits in cross-sectional studies. Neuroimage 50 (4), 1376–1383. [PubMed: 20109562]

Flynn SW, Lang DJ, Mackay AL, Goghari V, Vavasour IM, Whittall KP, et al., 2003 Abnormalities of myelination in schizophrenia detected in vivo with MRI, and post–mortem with analysis of oligodendrocyte proteins. Mol. Psychiatry 8 (9), 811–820. [PubMed: 12931208]

Gong T, Tong Q, He H, Sun Y, Zhong J, Zhang H, 2020 MTE-NODDI: multi-TE NODDI for disentangling non-T2-weighted signal fractions from compartment-specific T2 relaxation times. NeuroImage 217, 116906. [PubMed: 32387626]

Grussu F, Schneider T, Tur C, Yates RL, Tachrount M, Ianuş A, et al., 2017 Neurite dispersion: a new marker of multiple sclerosis spinal cord pathology? Ann. Clin. Transl. Neurol 4 (9), 663–679. [PubMed: 28904988]

Grussu F, Schneider T, Zhang H, Alexander DC, Wheeler-Kingshott CA, 2015 Neurite orientation dispersion and density imaging of the healthy cervical spinal cord in vivo. Neuroimage 111, 590–601. [PubMed: 25652391]

Guerrero JM, Adluru N, Bendlin BB, Goldsmith HH, Schaefer SM, Davidson RJ, et al., 2019 Optimizing the intrinsic parallel diffusivity in NODDI: an extensive empirical evaluation. PloS One 14 (9), e0217118. [PubMed: 31553719]

Gunning-Dixon FM, Brickman AM, Cheng JC, Alexopoulos GS, 2009 Aging of cerebral white matter: a review of MRI findings. Int. J. Geriatr. Psychiatry 24 (2), 109–117. [PubMed: 18637641]

Inano S, Takao H, Hayashi N, Abe O, Ohtomo K, 2011 Effects of age and gender on white matter integrity. AJNR Am. J. Neuroradiol 32 (11), 2103–2109. [PubMed: 21998104]

Jelescu IO, Veraart J, Adisetiyo V, Milla SS, Novikov DS, Fieremans E, 2015 One diffusion acquisition and different white matter models: how does microstructure change in human early development based on WMTI and NODDI? Neuroimage 107, 242–256. [PubMed: 25498427]

Kanaan NM, Pigino GF, Brady ST, Lazarov O, Binder LI, Morfini GA, 2013 Axonal degeneration in Alzheimer's disease: when signaling abnormalities meet the axonal transport system. Exp. Neurol 246, 44–53. [PubMed: 22721767]

Kodiweera C, Alexander AL, Harezlak J, McAllister TW, Wu YC, 2016 Age effects and sex differences in human brain white matter of young to middle-aged adults: a DTI, NODDI, and q-space study. Neuroimage 128, 180–192. [PubMed: 26724777]

Kolasinski J, Stagg CJ, Chance SA, Deluca GC, Esiri MM, Chang E-H, et al., 2012 A combined post-mortem magnetic resonance imaging and quantitative histological study of multiple sclerosis pathology. Brain: J. Neurol 135 (Pt 10), 2938–2951.

Kunz N, Zhang H, Vasung L, O'Brien KR, Assaf Y, Lazeyras F, et al., 2014 Assessing white matter microstructure of the newborn with multi-shell diffusion MRI and biophysical compartment models. Neuroimage 96, 288–299. [PubMed: 24680870]

Lankford CL, Does MD., 2013 On the inherent precision of mcDESPOT. Magn. Resonance Med 69 (1), 127–136.

Laule C, Kozlowski P, Leung E, Li DK, Mackay AL, Moore GR, 2008 Myelin water imaging of multiple sclerosis at 7 T: correlations with histopathology. NeuroImage 40 (4), 1575–1580. [PubMed: 18321730]

Laule C, Leung E, Lis DK, Traboulsee AL, Paty DW, MacKay AL, et al., 2006 Myelin water imaging in multiple sclerosis: quantitative correlations with histopathology. Multiple Scler. (Houndmills, Basingstoke, England) 12 (6), 747–753.

Laule C, Vavasour IM, Moore GR, Oger J, Li DK, Paty DW, et al., 2004 Water content and myelin water fraction in multiple sclerosis. A T2 relaxation study. J. Neurol 251 (3), 284–293. [PubMed: 15015007]

MacKay A, Whittall K, Adler J, Li D, Paty D, Graeb D, 1994 In vivo visualization of myelin water in brain by magnetic resonance. Magn. Resonance Med 31 (6), 673–677.

MacKay AL, Laule C, 2016 Magnetic resonance of myelin water: an in vivo marker for myelin. Brain Plasticity 2 (1), 71–91. [PubMed: 29765849]

MacKay AL, Vavasour IM, Rauscher A, Kolind SH, Madler B, Moore GR, et al., 2009 MR relaxation in multiple sclerosis. Neuroimaging Clin. North Am 19 (1), 1–26.

Marner L, Nyengaard JR, Tang Y, Pakkenberg B, 2003 Marked loss of myelinated nerve fibers in the human brain with age. J. Comp. Neurol 462 (2), 144–152. [PubMed: 12794739]

Medana IM, Esiri MM, 2003 Axonal damage: a key predictor of outcome in human CNS diseases. Brain: J. Neurol 126 (3), 515–530.

Mensch S, Baraban M, Almeida R, Czopka T, Ausborn J, El Manira A, et al., 2015 Synaptic vesicle release regulates myelin sheath number of individual oligodendrocytes in vivo. Nat. Neurosci 18 (5), 628–630. [PubMed: 25849985]

Merluzzi AP, Dean DC 3rd, Adluru N, Suryawanshi GS, Okonkwo OC, Oh JM, et al., 2016 Age-dependent differences in brain tissue microstructure assessed with neurite orientation dispersion and density imaging. Neurobiol. Aging 43, 79–88. [PubMed: 27255817]

Merluzzi AP, Dean DC 3rd, Adluru N, Suryawanshi GS, Okonkwo OC, Oh JM, et al., 2016 Age-dependent differences in brain tissue microstructure assessed with neurite orientation dispersion and density imaging. Neurobiol Aging 43, 79–88. [PubMed: 27255817]

Mitchell T, Archer DB, Chu WT, Coombes SA, Lai S, Wilkes BJ, et al., 2019 Neurite orientation dispersion and density imaging (NODDI) and free-water imaging in Parkinsonism. Hum. Brain Mapp 40 (17), 5094–5107. [PubMed: 31403737]

Mohammadi S, Moller HE, Kugel H, Muller DK, Deppe M, 2010 Correcting eddy current and motion effects by affine whole-brain registrations: evaluation of three-dimensional distortions and comparison with slicewise correction. Magn. Reson. Med 64 (4), 1047–1056. [PubMed: 20574966]

Nazeri A, Chakravarty MM, Rotenberg DJ, Rajji TK, Rathi Y, Michailovich OV, et al., 2015 Functional consequences of neurite orientation dispersion and density in humans across the adult lifespan. J. Neurosci 35 (4), 1753–1762. [PubMed: 25632148]

Okubo G, Okada T, Yamamoto A, Fushimi Y, Okada T, Murata K, et al., 2017 Relationship between aging and T1 relaxation time in deep gray matter: a voxel-based analysis. J. Magn. Resonance Imaging: JMRI 46 (3), 724–731.

Pannese E, 2011 Morphological changes in nerve cells during normal aging. Brain Struct. Funct 216 (2), 85–89. [PubMed: 21431333]

Peters A, 2002 The effects of normal aging on myelin and nerve fibers: a review. J. Neurocytol 31 (8–9), 581–593. [PubMed: 14501200]

Raz N, 2000 Aging of the brain and its impact on cognitive performance: integration of structural and functional findings In: The Handbook of Aging and Cognition. Lawrence Erlbaum Associates Publishers, Mahwah, NJ, US, pp. 1–90.

Saito N, Sakai O, Ozonoff A, Jara H, 2009 Relaxo-volumetric multispectral quantitative magnetic resonance imaging of the brain over the human lifespan: global and regional aging patterns. Magn. Resonance Imaging 27 (7), 895–906.

Shock N, 1985 Normal human aging: the Baltimore longitudinal study of aging. J. Gerontol 40 (6), 767–774.

Simons M, Nave K-A, 2015 Oligodendrocytes: myelination and axonal support. Cold Spring Harbor Perspect. Biol 8 (1) a020479-a.

Sirrs SM, Laule C, Madler B, Brief EE, Tahir SA, Bishop C, et al., 2007 Normal-appearing white matter in patients with phenylketonuria: water content, myelin water fraction, and metabolite concentrations. Radiology 242 (1), 236–243. [PubMed: 17185670]

Smith CM, Cooksey E, Duncan ID, 2013 Myelin loss does not lead to axonal degeneration in a long-lived model of chronic demyelination. J. Neurosci. : Off. J. Soc. Neurosci 33 (6), 2718–2727.

Stassart RM, Möbius W, Nave K-A, Edgar JM, 2018 The axon-myelin unit in development and degenerative disease. Front. Neurosci 12 (467).

Stollberger R, Wach P, 1996 Imaging of the active B1 field in vivo. Magn. Resonance Med 35 (2), 246–251.

Stricker NH, Schweinsburg BC, Delano-Wood L, Wierenga CE, Bangen KJ, Haaland KY, et al., 2009 Decreased white matter integrity in late-myelinating fiber pathways in Alzheimer's disease supports retrogenesis. NeuroImage 45 (1), 10–16. [PubMed: 19100839]

Sullivan EV, Pfefferbaum A, 2006 Diffusion tensor imaging and aging. Neurosci. Biobehav. Rev 30 (6), 749–761. [PubMed: 16887187]

Tang Y, Nyengaard JR, Pakkenberg B, Gundersen HJ, 1997 Age-induced white matter changes in the human brain: a stereological investigation. Neurobiol. Aging 18 (6), 609–615. [PubMed: 9461058]

Timmers I, Roebroeck A, Bastiani M, Jansma B, Rubio-Gozalbo E, Zhang H, 2016 Assessing microstructural substrates of white matter abnormalities: a comparative study using DTI and NODDI. PLoS One 11 (12), e0167884. [PubMed: 28002426]

Timmers I, Zhang H, Bastiani M, Jansma BM, Roebroeck A, Rubio-Gozalbo ME, 2015 White matter microstructure pathology in classic galactosemia revealed by neurite orientation dispersion and density imaging. J. Inherit. Metab. Dis 38 (2), 295–304. [PubMed: 25344151]

Wake H, Lee PR, Fields RD, 2011 Control of local protein synthesis and initial events in myelination by action potentials. Sci. (New York, NY) 333 (6049), 1647–1651.

Wen Q, Kelley DA, Banerjee S, Lupo JM, Chang SM, Xu D, et al., 2015 Clinically feasible NODDI characterization of glioma using multiband EPI at 7 T. Neuroimage Clin. 9, 291–299. [PubMed: 26509116]

West DJ, Teixeira RPAG, Wood TC, Hajnal JV, Tournier J-D, Malik SJ, 2019 Inherent and unpredictable bias in multi-component DESPOT myelin water fraction estimation. NeuroImage 195, 78–88. [PubMed: 30930311]

Westlye LT, Walhovd KB, Dale AM, Bjornerud A, Due-Tonnessen P, Engvig A, et al., 2010 Life-span changes of the human brain white matter: diffusion tensor imaging (DTI) and volumetry. Cereb Cortex 20 (9), 2055–2068. [PubMed: 20032062]

Winston GP, Micallef C, Symms MR, Alexander DC, Duncan JS, Zhang H, 2014 Advanced diffusion imaging sequences could aid assessing patients with focal cortical dysplasia and epilepsy. Epilepsy Res. 108 (2), 336–339. [PubMed: 24315018]

Winston GP., 2015 The potential role of novel diffusion imaging techniques in the understanding and treatment of epilepsy. Quant. Imaging Med. Surgery 5 (2), 279–287.

Yeatman JD, Wandell BA, Mezer AA, 2014 Lifespan maturation and degeneration of human brain white matter. Nat. Commun 5, 4932. [PubMed: 25230200]

Zhang H, Schneider T, Wheeler-Kingshott CA, Alexander DC, 2012 NODDI: practical in vivo neurite orientation dispersion and density imaging of the human brain. NeuroImage 61 (4), 1000–1016. [PubMed: 22484410]

Zhang J, Kolind SH, Laule C, MacKay AL, 2015 Comparison of myelin water fraction from multiecho T2 decay curve and steady-state methods. Magn. Resonance Med 73 (1), 223–232.

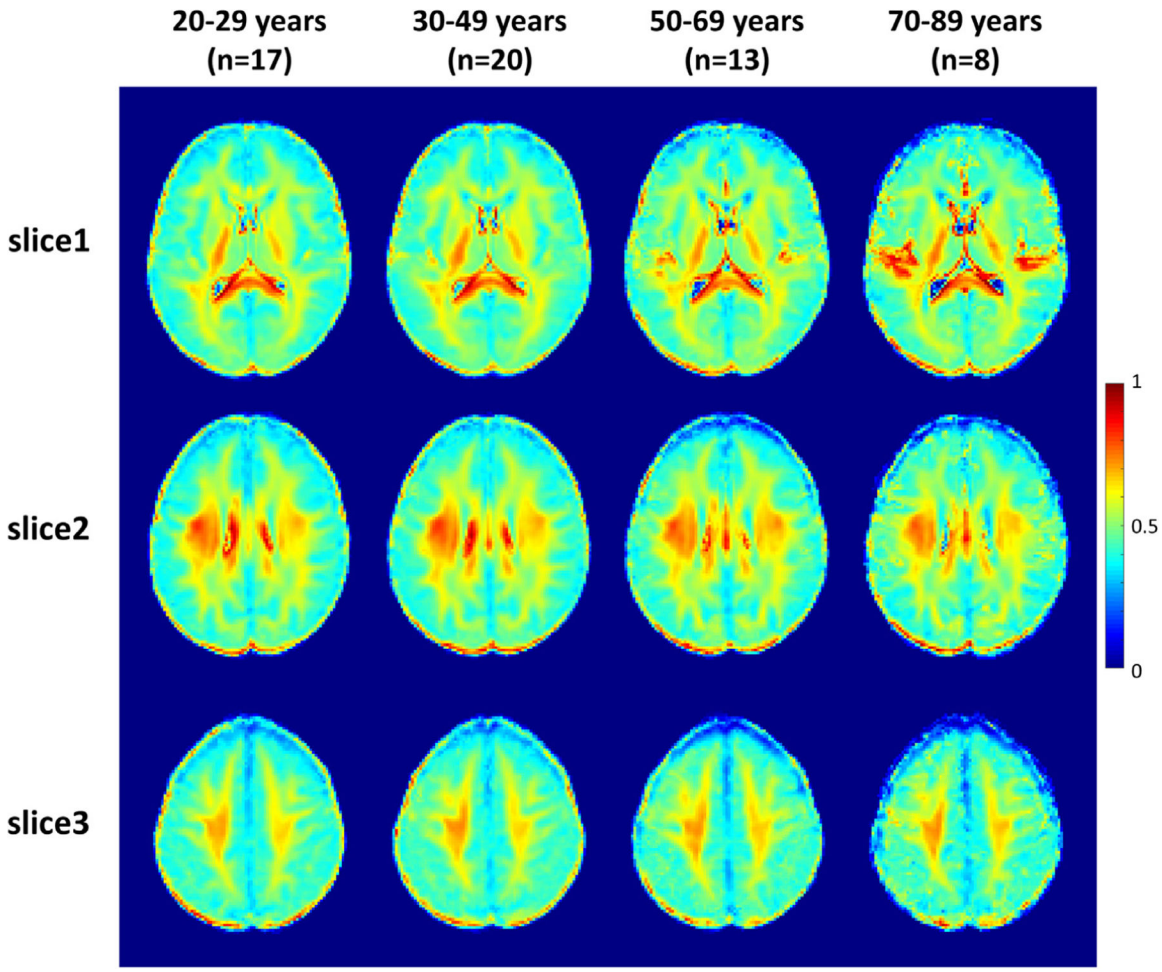

Fig. 1.

Neurite density index (NDI) maps represented as averaged participant maps calculated over age intervals. Results are shown for three representative slices. Visual inspection of NDI maps shows that NDI follow complex patterns with age with most regions exhibiting an increase in NDI values from early age until middle age followed by a more rapid decrease in several brain regions, while other regions exhibiting constant patterns.

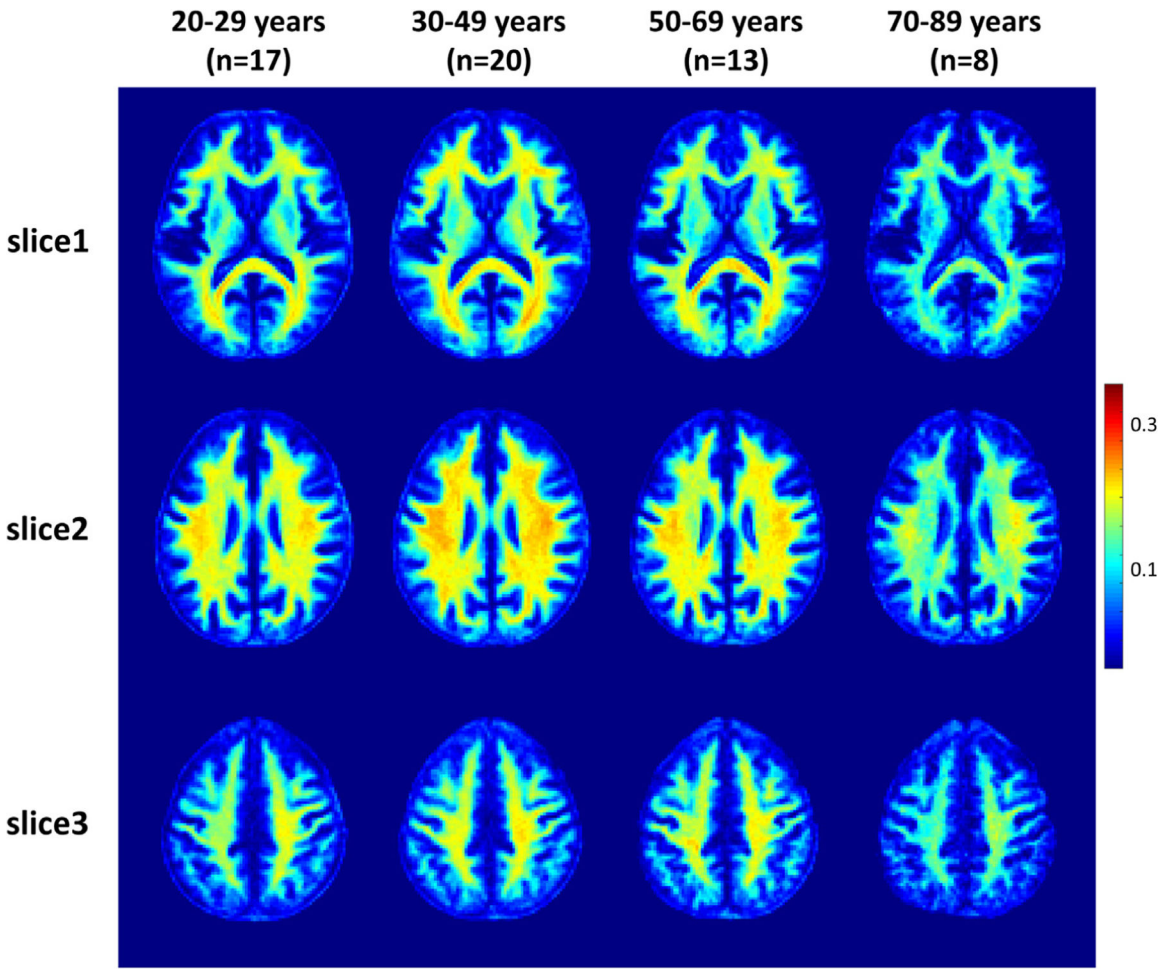

Fig. 2.

Myelin water fraction (MWF) represented as averaged participant maps calculated over age intervals. Results are shown for three representative slices. Visual inspection of MWF maps shows an increase in MWF values from early age until middle age followed by a more rapid decrease in several brain regions. This suggests progressive myelination continuing into middle age followed by a decline in myelin content at older ages.

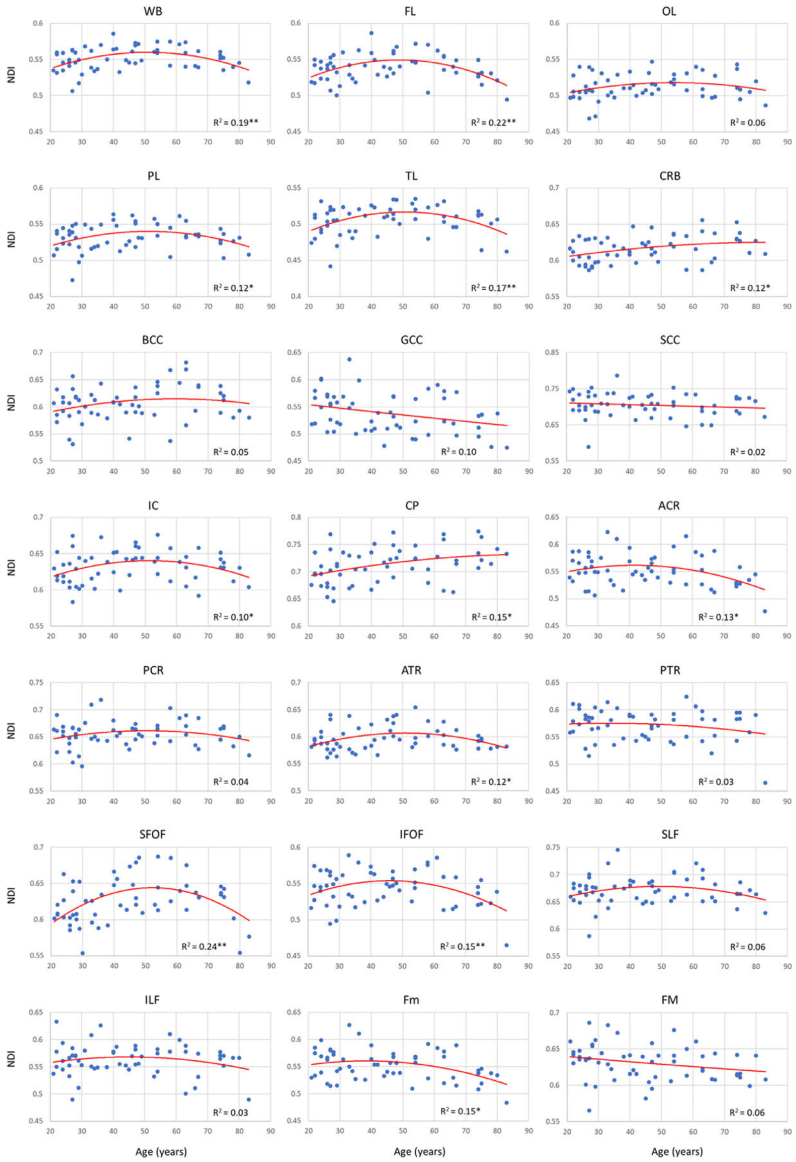

Fig. 3.

Regional neurite density index (NDI) trends as a function of age. For each ROI, the coefficient of determination, R^2, is reported and * represents the significance of the overall model after FDR correction with * $p < 0.05$ or ** $p < 0.01$. Several regions investigated show an inverted U-shaped trend of NDI with age, while other regions showed constant or decreasing associations with age. WB: whole brain white matter, FL: frontal lobes, PL: parietal lobes, TL: temporal lobes, OL: occipital lobes, CRB: cerebellum, BCC: body of corpus callosum, GCC: genu of corpus callosum, SCC: splenium of corpus callosum, IC: internal capsules, CP: cerebral peduncle, ACR: anterior corona radiata, PCR: posterior corona radiata, ATR: anterior thalamic radiation, PTR: posterior thalamic radiation, IFOF: inferior fronto-occipital fasciculus, SFOF: superior fronto-occipital fasciculus, ILF: inferior longitudinal fasciculus, SLF: superior longitudinal fasciculus, Fm: forceps minor, FM: forceps major.

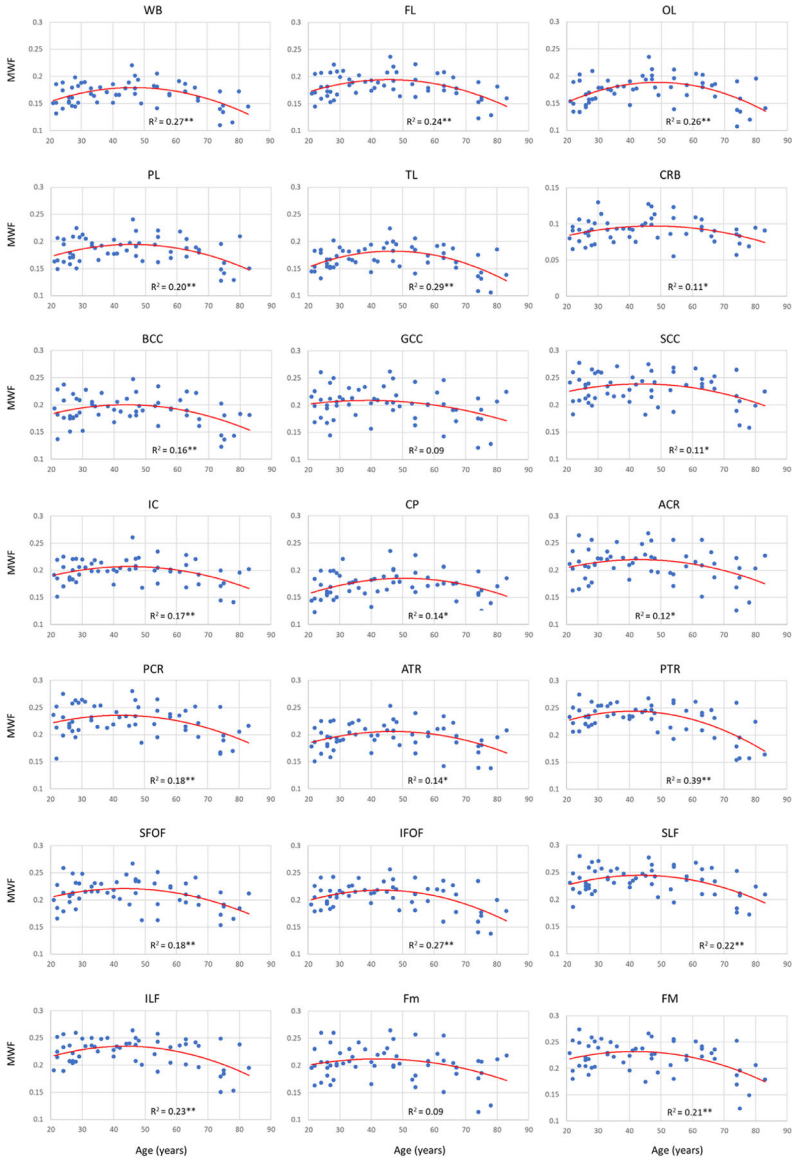

Fig. 4.

Regional myelin water fraction (MWF) trends as a function of age. For each ROI, the coefficient of determination, R^2, is reported and * represents the significance of the overall model after FDR correction with * $p < 0.05$ or ** $p < 0.01$. All regions investigated show an inverted U-shaped trend of MWF with age, but with differences in detail between regions. WB: whole brain white matter, FL: frontal lobes, PL: parietal lobes, TL: temporal lobes, OL: occipital lobes, CRB: cerebellum, BCC: body of corpus callosum, GCC: genu of corpus callosum, SCC: splenium of corpus callosum, IC: internal capsules, CP: cerebral peduncle, ACR: anterior corona radiata, PCR: posterior corona radiata, ATR: anterior thalamic radiation, PTR: posterior thalamic radiation, IFOF: inferior fronto-occipital fasciculus, SFOF: superior fronto-occipital fasciculus, ILF: inferior longitudinal fasciculus, SLF: superior longitudinal fasciculus, Fm: forceps minor, FM: forceps major.

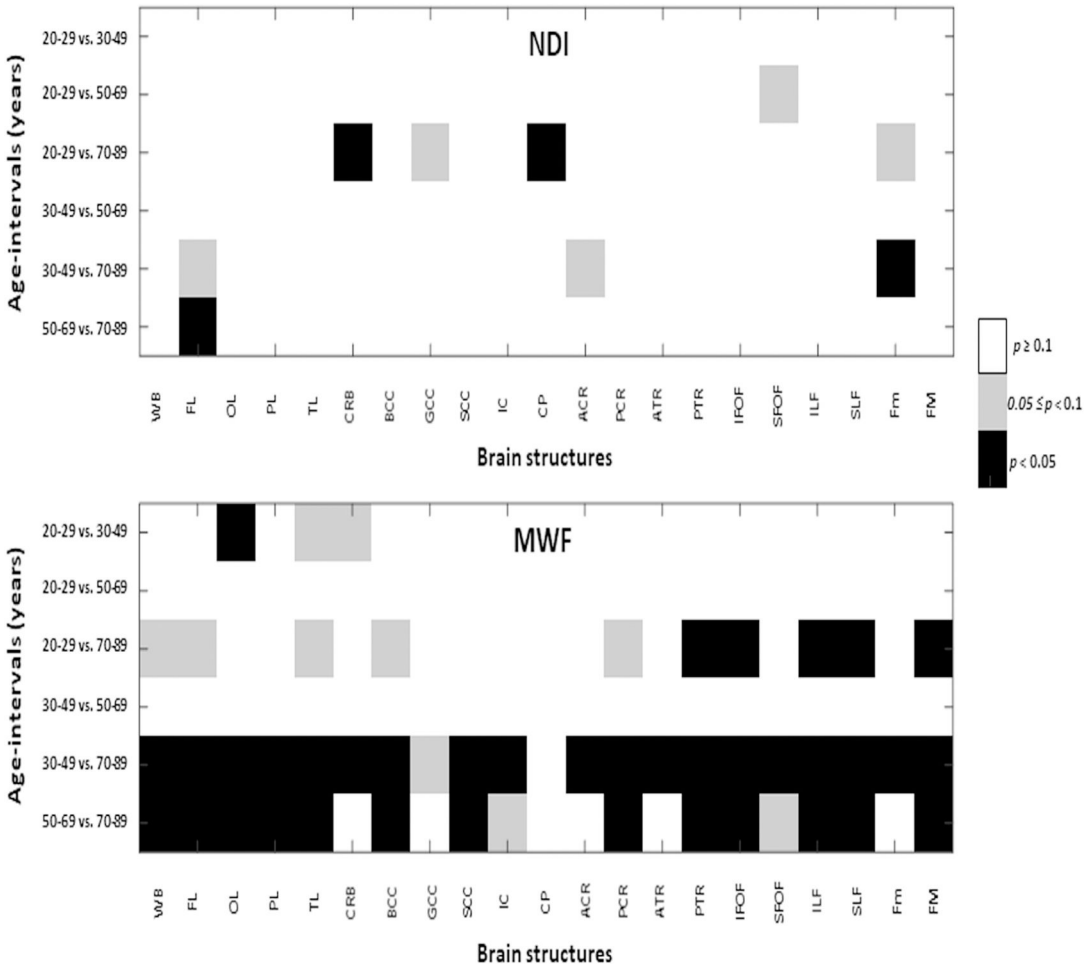

Fig. 5.

Post hoc family-wise error (Bonferroni) correction of the ANOVA results. A black square indicates a post-correction significant difference between the two corresponding age groups in mean NDI (top panel) or mean MWF (bottom panel), a gray square indicates a post-correction close to significant difference, for each ROI, while a white squares indicate non significance. For example, in FL, there were post-correction statistically significant differences between the age intervals 50–69 and 70–89 in NDI and MWF. WB: whole brain white matter, FL: frontal lobes, PL: parietal lobes, TL: temporal lobes, OL: occipital lobes, CRB: cerebellum, BCC: body of corpus callosum, GCC: genu of corpus callosum, SCC: splenium of corpus callosum, IC: internal capsules, CP: cerebral peduncle, ACR: anterior corona radiata, PCR: posterior corona radiata, ATR: anterior thalamic radiation, PTR: posterior thalamic radiation, IFOF: inferior fronto-occipital fasciculus, SFOF: superior fronto-occipital fasciculus, ILF: inferior longitudinal fasciculus, SLF: superior longitudinal fasciculus, Fm: forceps minor, FM: forceps major.

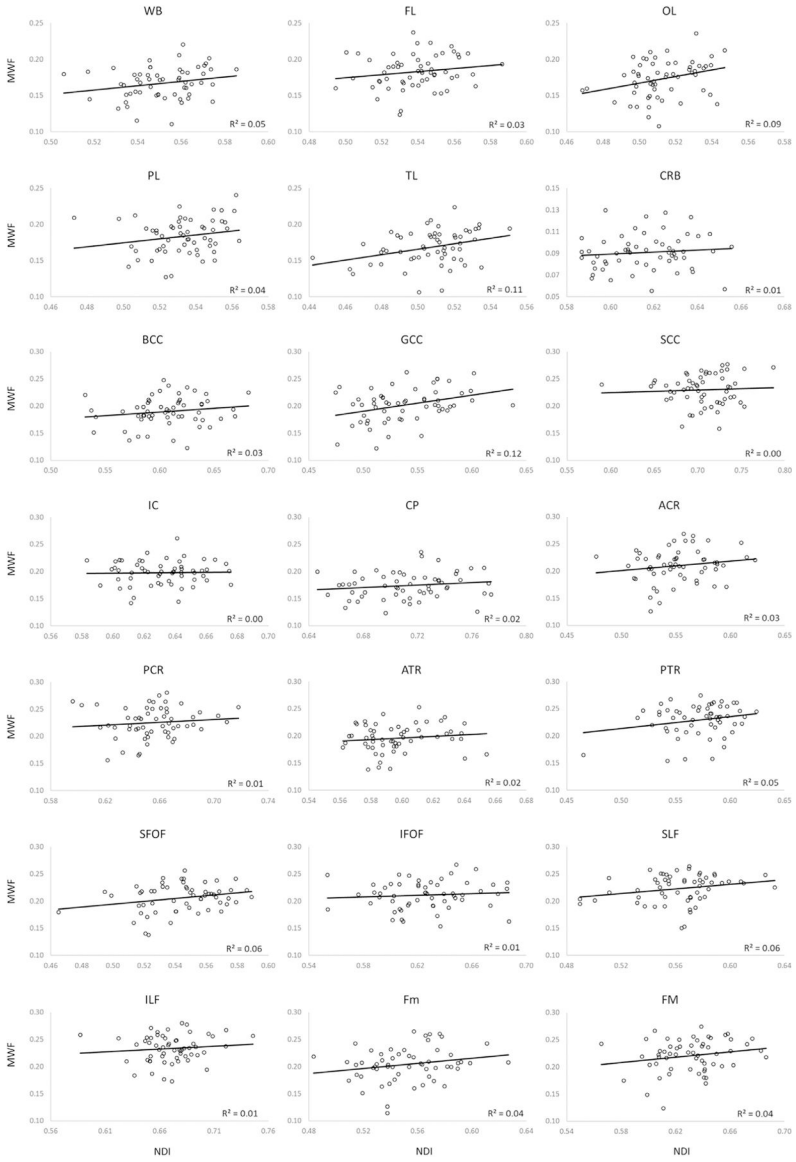

Fig. 6.

Pearson correlation between MWF and NDI in 21 WM ROIs. R^2 denotes the coefficient of determination. None of the correlations were statistically significant. WB: whole brain white matter, FL: frontal lobes, PL: parietal lobes, TL: temporal lobes, OL: occipital lobes, CRB: cerebellum, BCC: body of corpus callosum, GCC: genu of corpus callosum, SCC: splenium of corpus callosum, IC: internal capsules, CP: cerebral peduncle, ACR: anterior corona radiata, PCR: posterior corona radiata, ATR: anterior thalamic radiation, PTR: posterior thalamic radiation, IFOF: inferior fronto-occipital fasciculus, SFOF: superior fronto-occipital fasciculus, ILF: inferior longitudinal fasciculus, SLF: superior longitudinal fasciculus, Fm: forceps minor, FM: forceps major.

Table 1

Significance of each coefficient incorporated into the linear regression analysis of NDI and MWF, and year of apparent maximum in each ROI. NA indicates "not applicable" for a non-significant age^2 term. * indicates $p < 0.05$, ** indicates $p < 0.01$, + indicates $p < 0.1$, and - indicates non-significant effects. All p-values presented are obtained after FDR correction.

	NDI Age	Sex	Age^2	Year of max NDI	MWF Age	Sex	Age^2	Year of max MWF
WB	−	−	* *	50.9	−	−	* *	46.6
FL	−	−	* *	48.8	+	−	* *	45.5
OL	−	−	−	NA	−	−	* *	48.7
PL	−	−	*	51.0	−	−	* *	46.8
TL	−	−	*	50.5	−	−	* *	45.7
CRB	*	−	−	NA	−	−	*	47.6
BCC	−	−	−	NA	+	−	*	43.7
GCC	*	−	−	NA	+	−	−	NA
SCC	−	−	−	NA	−	−	*	43.7
IC	−	−	+	51.3	−	−	* *	45.0
CP	*	−	−	NA	−	−	* *	50.4
ACR	−	−	+	41.6	−	−	*	43.2
PCR	−	−	−	NA	*	−	*	42.2
ATR	−	−	*	50.7	−	−	* *	46.8
PTR	−	−	−	NA	* *	−	* *	40.8
SFOF	−	−	* *	52.2	+	−	*	43.3
IFOF	−	−	*	46.0	*	−	* *	43.3
SLF	−	−	−	NA	*	−	* *	43.5
ILF	−	−	−	NA	*	−	* *	43.6
Fm	−	−	−	NA	−	−	+	42.1
FM	*	−	−	NA	*	−	*	41.6

MWF: myelin water fraction, NDI: neurite density index, WB: whole brain, FL: frontal lobes, PL: parietal lobes, TL: temporal lobes, OL: occipital lobes, CRB: cerebellum, BCC: body of corpus callosum, GCC: genu of corpus callosum, SCC: splenium of corpus callosum, IC: internal capsules, CP: cerebral peduncle, ACR: anterior corona radiata, PCR: posterior corona radiata, ATR: anterior thalamic radiation, PTR: posterior thalamic radiation, IFOF: inferior fronto-occipital fasciculus, SFOF: superior fronto-occipital fasciculus, ILF: inferior longitudinal fasciculus, SLF: superior longitudinal fasciculus, Fm: forceps minor, FM: forceps major.